Science Advances
AAAS

advances.sciencemag.org/cgi/content/full/6/36/eabc3296/DC1

Supplementary Materials for

On-site identification of ozone damage in fruiting plants using vapor-deposited conducting polymer tattoos

Jae Joon Kim, Ruolan Fan, Linden K. Allison, Trisha L. Andrew*

*Corresponding author. Email: tandrew@umass.edu

Published 4 September 2020, *Sci. Adv.* **6**, eabc3296 (2020)
DOI: 10.1126/sciadv.abc3296

This PDF file includes:

Additional Methods

Relative Water Content

The relative water content (RWC) of a leaf was calculated using equation 1:

$$\text{RWC } (\%) = \frac{Fresh\ Weight - Dry\ Weight}{Turgid\ Weight - Dry\ Weight} \times 100\ (\%) \qquad (1)$$

The dry weight was determined after each leaf was heated at 50 °C for 5 days, when the mass became constant. The turgid weight was measured after immersing fresh leaves in distilled water for 5 hours in the dark and removing extra water on the surface with Texwipes.

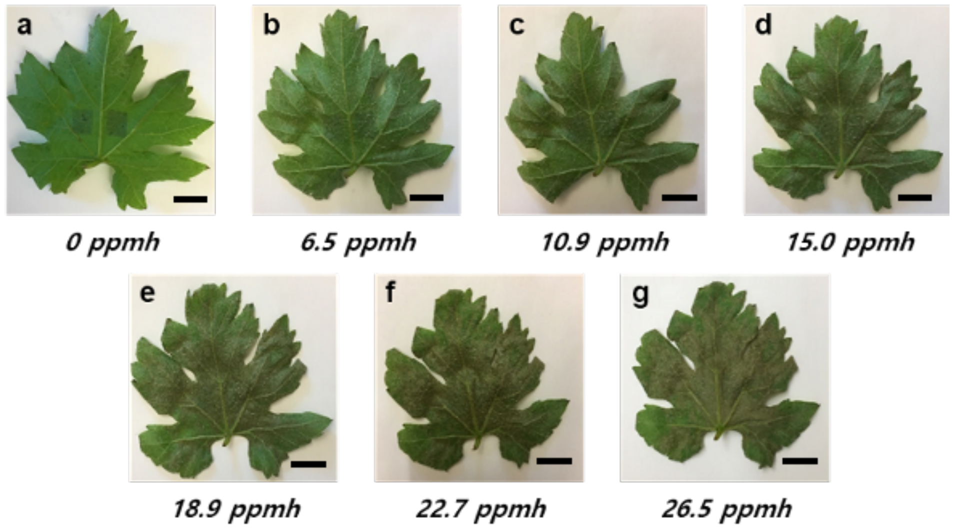

Fig. S1. **Effects of ozone exposure**. Images of underside (abaxial side) of a grape leaf after exposure to increasing doses of ozone. The scale bars are 10 mm. The vapor-deposited PEDOT-Cl electrode ("tattoo") is clearly visible in the 0 ppmh image. Photo Credit: Dr. Jae Joon Kim, University of Massachusetts Amherst.

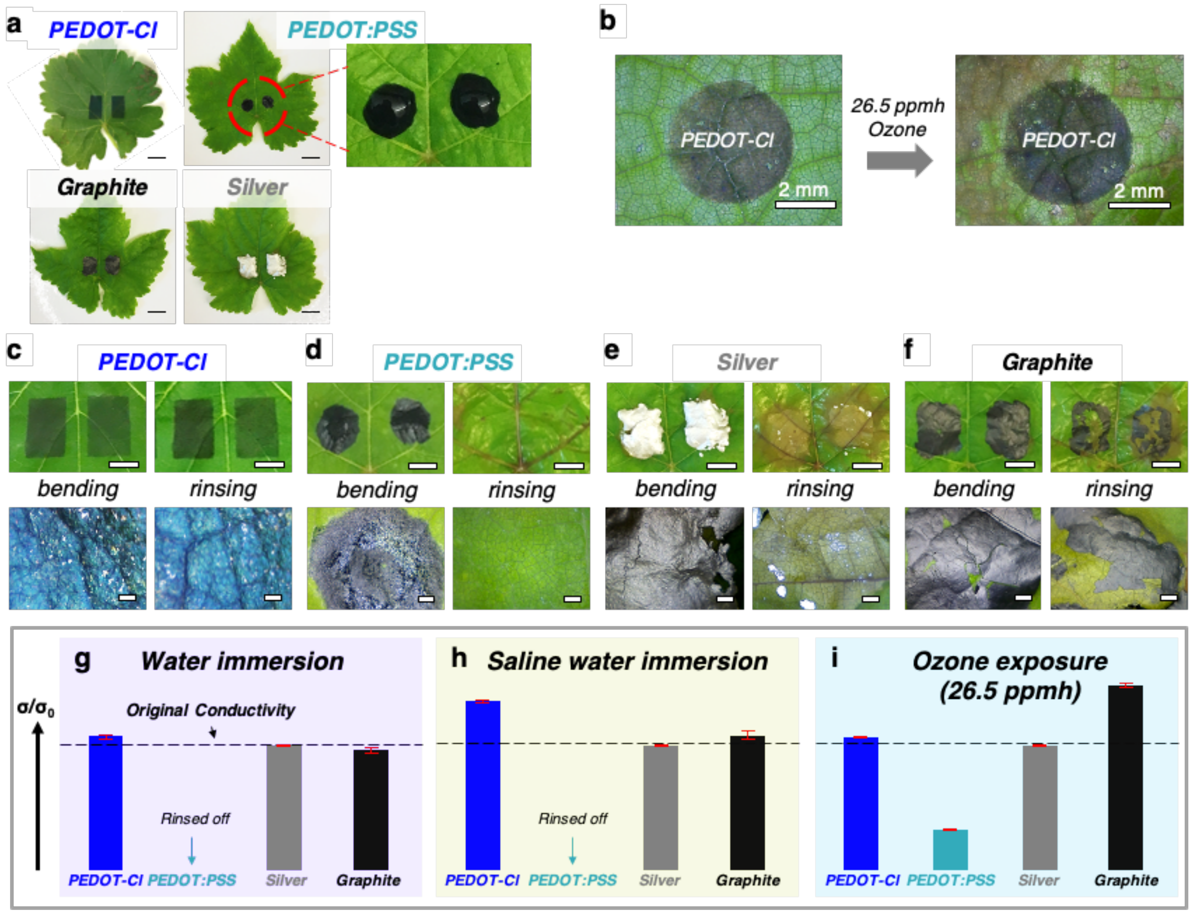

Fig. S2. **Comparison of electrode materials**. **a**, Images of electrodes on grape leaves. The scale bars are 10 mm. The expansion shows a picture of the as-deposited PEDOT:PSS droplet on the hydrophobic surface of grape leaf. **b**, Picture of the PEDOT-Cl tattoo before and after exposure to ozone. **c-f**, Magnified images of the electrodes on the leaf after bending and rinsing treatment. The scale bars are 5 mm (top row) and 1 mm (bottom row). **g-i**, Comparison of relative conductivity change after water, saline water and ozone exposure. Photo Credit: Dr. Jae Joon Kim, University of Massachusetts Amherst.

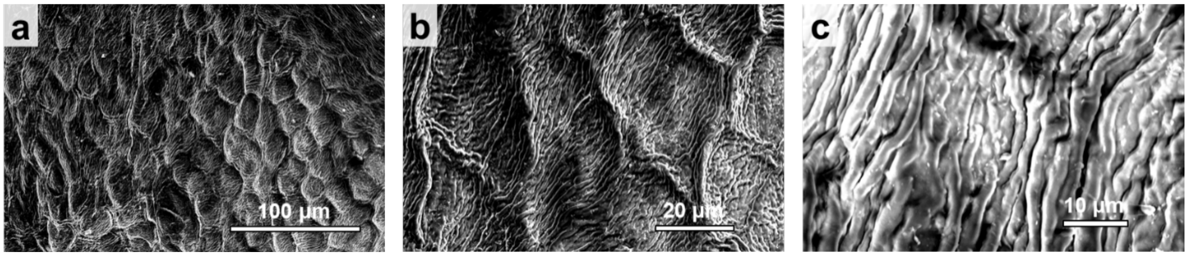

Fig. S3. Investigating the surface of a grape leaf. SEM images of the surface of a grape leaf.

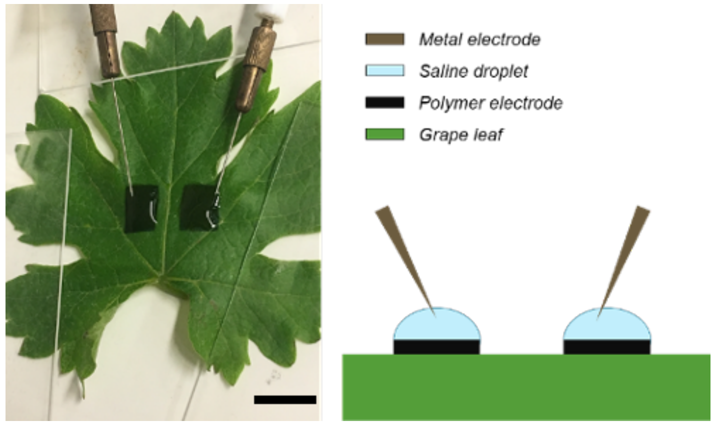

Fig. S4. Measurement setup. Picture and scheme of a typical impedance measurement on an electrode decorated grape leaf. The scale bar is 10 mm. Photo Credit: Dr. Jae Joon Kim, University of Massachusetts Amherst.

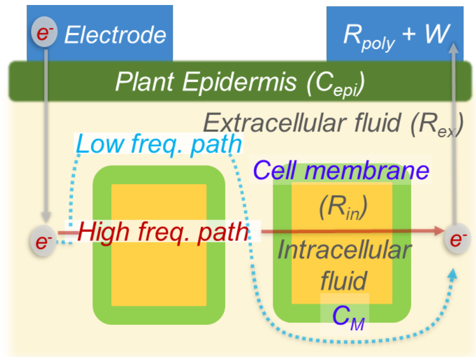

Fig. S5. **Conduction pathways in a representative leaf**. Scheme of the conduction pathways operating at different bias frequencies during an impedance measurement.

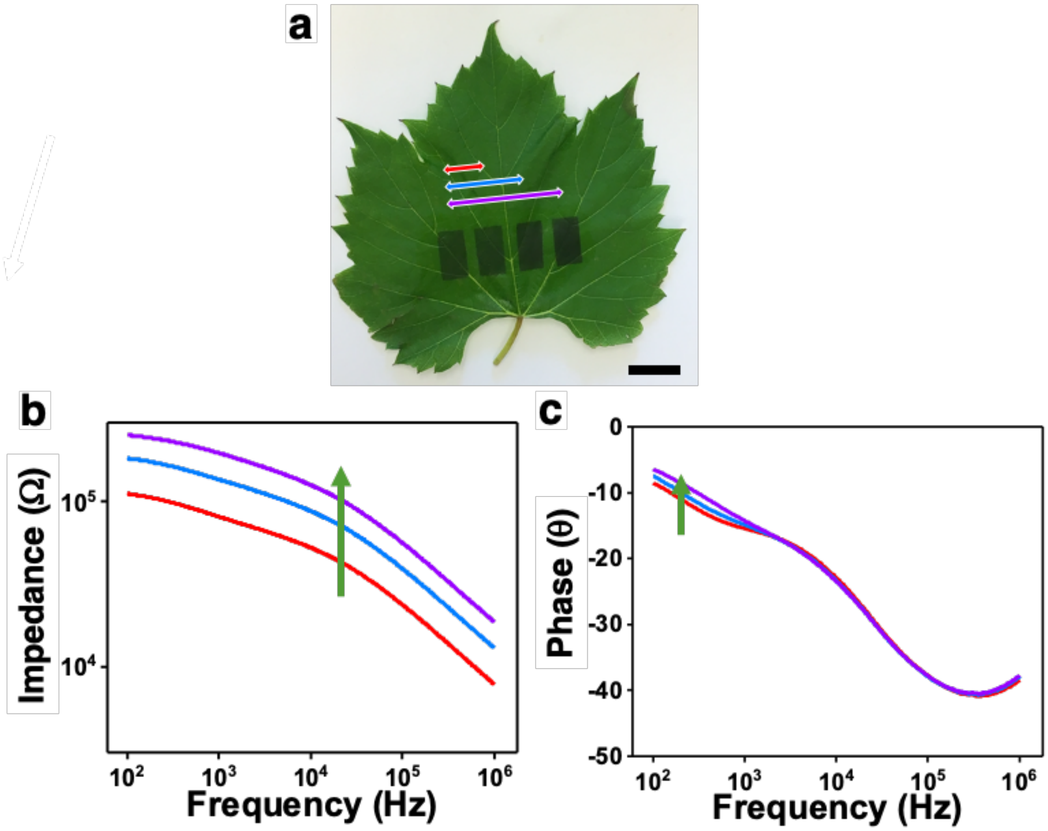

Fig. S6. **Effect of electrode dimensions on impedance spectra of a grape leaf**. **a**, Image of electrodes on the grape leaf. The scale bar is 10 mm. Photo Credit: Dr. Jae Joon Kim, University of Massachusetts Amherst. **b**, impedance and **c**, phase as a function of frequency.

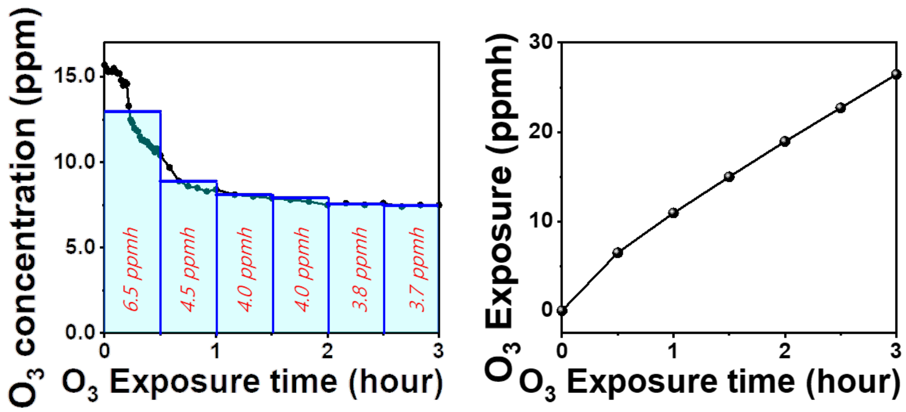

Fig. S7. **Calibrating ozone dose**. Calibration curve for obtaining ozone dose (ppmh) as a function of exposure time inside an ozone generation chamber.

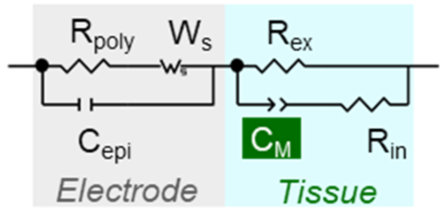

Fig. S8. **The equivalent electrical circuit used to model impedance data**. The equivalent circuit contains components arising from the electrode and leaf tissue.

Table S1. **Extracted values from circuit modelling**. Extracted values, percent error for each circuit component and the corresponding fitting accuracy (chi-square).

Ozone exposure	Element		Electrode part					Tissue part					Chi-square
			R_{poly} (Ω)	A_W (Ω)	B_W (s)	p	C_{epi} (F)	R_{ex} (Ω)	R_{in} (Ω)	Y_0	p	C_m (F)	
0 ppmh	Value	(Ω, F)	1.1.E+04	1.4.E+05	1.1.E-03	3.2.E-01	1.7.E-10	3.3.E+04	4.2.E+03	4.2.E-09	6.6.E-01	4.6.E-11	1.8.E-06
	Error	(%)	2.0.E+00	8.9.E-01	1.8.E+00	5.1.E-01	1.7.E+00	1.4.E+00	5.2.E-01	2.2.E+00	2.0.E-01	-	
6.5 ppmh	Value	(Ω, F)	1.2.E+04	1.1.E+05	1.1.E-03	3.4.E-01	2.0.E-10	3.3.E+04	4.7.E+03	5.3.E-09	6.4.E-01	4.5.E-11	1.4.E-06
	Error	(%)	9.2.E-01	7.0.E-01	1.4.E+00	3.8.E-01	1.3.E+00	1.1.E+00	4.7.E-01	2.3.E+00	2.1.E-01	-	
10.9 ppmh	Value	(Ω, F)	9.9.E+03	9.2.E+04	7.4.E-03	3.4.E-01	2.2.E-10	3.8.E+04	5.8.E+03	7.8.E-09	6.1.E-01	4.7.E-11	1.7.E-06
	Error	(%)	1.4.E+00	8.5.E-01	1.3.E+00	4.4.E-01	1.8.E+00	1.3.E+00	5.8.E-01	3.1.E+00	3.0.E-01	-	
15.0 ppmh	Value	(Ω, F)	6.2.E+03	8.6.E+04	6.4.E-04	3.6.E-01	2.5.E-10	4.7.E+04	8.5.E+03	1.3.E-08	5.5.E-01	3.6.E-11	1.7.E-06
	Error	(%)	2.9.E+00	9.7.E-01	1.2.E+00	4.5.E-01	2.2.E+00	1.5.E+00	7.8.E-01	4.5.E+00	4.8.E-01	-	
18.9 ppmh	Value	(Ω, F)	2.7.E+03	7.0.E+04	5.4.E-04	3.8.E-01	2.5.E-10	7.1.E+04	1.1.E+04	4.9.E-08	4.4.E-01	4.3.E-11	2.3.E-06
	Error	(%)	4.1.E+00	2.1.E+00	1.5.E+00	7.8.E-01	2.2.E+00	2.0.E+00	1.6.E+00	7.8.E+00	1.1.E+00	-	
22.7 ppmh	Value	(Ω, F)	5.2.E+03	1.5.E+05	8.9.E-04	3.8.E-01	8.5.E-11	6.2.E+04	7.9.E+03	6.7.E-08	3.6.E-01	4.8.E-12	5.0.E-06
	Error	(%)	1.9.E+00	1.6.E+00	2.1.E+00	6.9.E-01	2.0.E+00	2.8.E+00	1.5.E+01	2.3.E+01	4.0.E+00	-	
26.5 ppmh	Value	(Ω, F)	7.0.E+03	1.6.E+05	8.0.E-04	3.8.E-01	7.9.E-11	5.4.E+04	2.0.E+04	9.6.E-09	4.7.E-01	2.7.E-12	4.8.E-06
	Error	(%)	3.2.E+00	8.5.E-01	1.4.E+00	4.2.E-01	1.8.E+00	1.7.E+00	6.0.E+00	2.3.E+01	2.9.E+00	-	

The equivalent electrical circuit model is comprised of an electrode part and tissue components, as previously reported by our research group (*47*). Electrode parts include a resistor, R_{poly}, that represents the intrinsic conductivity of the PEDOT-Cl electrode, a capacitor, C_{epi}, that accounts for the capacitance introduced at the interface between the electrode and the insulating leaf epidermis, and a transmissive Warburg component, W_s, that stands for ion diffusion between the polymer coating and leaf cells. The Warburg component is further comprised of three subparts: a diffusion impedance constant, A_W, a Warburg exponent, p, and a characteristic ion diffusion time, B_W. Additional circuit components for the saline droplet were not necessary to accurately fit the recorded data in the frequency range used in this study. The Hayden model (*49*) was used to translate three principal cellular components of a grape leaf into discrete circuit elements: extracellular fluid was represented by a resistor, R_{ex}; intracellular fluid was represented by a resistor, R_{in}; and the cell membrane was represented by capacitor, C_M. The cell membrane capacitance was represented in the circuit as a constant phase element (CPE) instead of a simple capacitor because leaf tissue is composed of an ensemble of cells that result in electronic dispersity. The value for C_M was calculated using Equation 2 (*48,50*):

$$C_M = Y_0^{\frac{1}{p}}(R_{in} + R_{ex})^{\frac{1-p}{p}} \quad (2)$$

where Y_0 is the CPE constant and p is the CPE exponent.

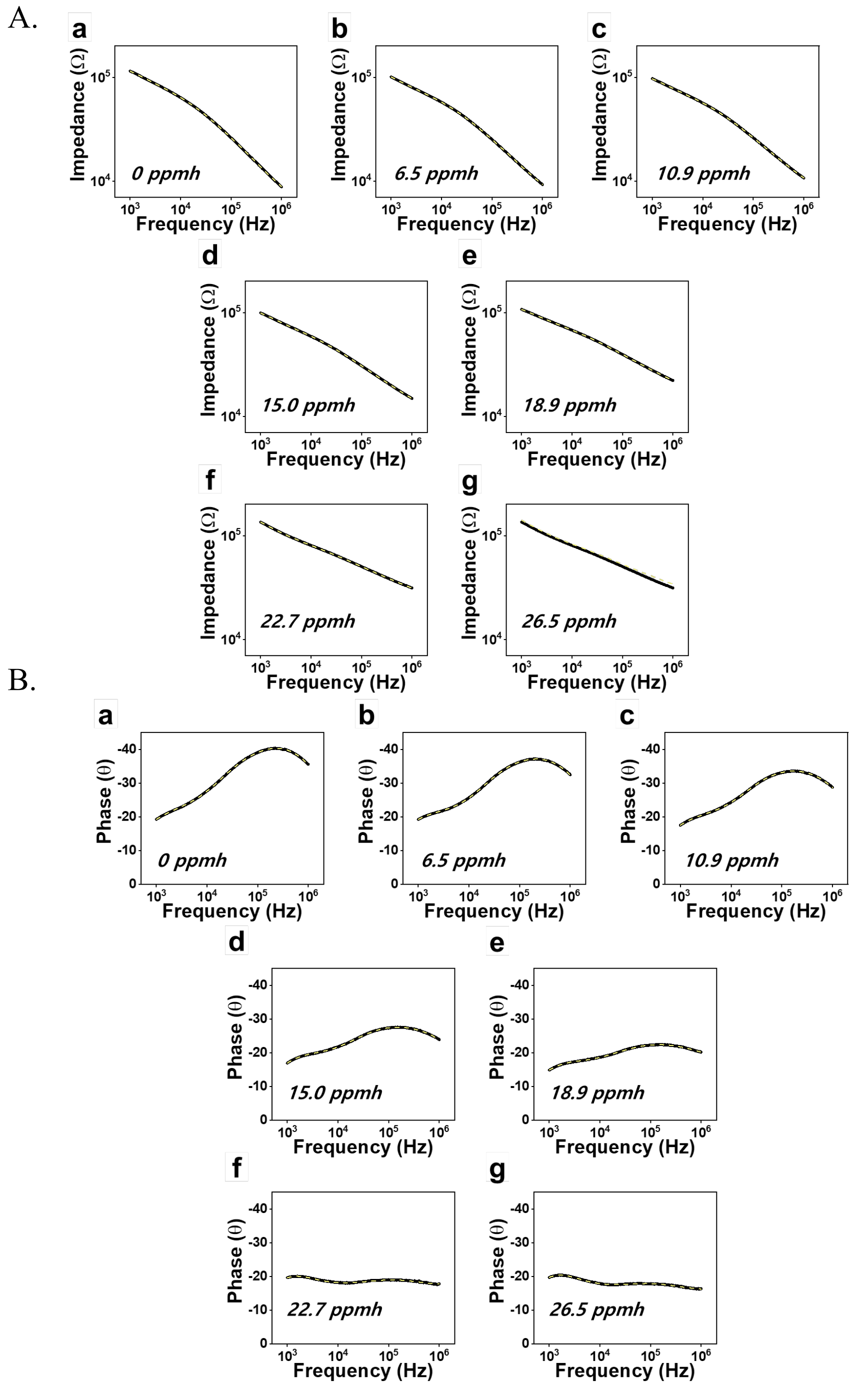

Fig. S9. **A**. **Comparison of the impedance-frequency relationship between the measured data and the fitting curve**. The measured data is plotted with a solid black line and the fitting curve based on the equivalent model circuit is plotted as a dotted line. **B.** Comparison of the phase-frequency relationship between the measured data and the fitting curve. The measured data is plotted with a solid black line and the fitting curve based on the equivalent model circuit is plotted as a dotted line.

REFERENCES AND NOTES

1. H. Pleijel, M. C. Broberg, J. Uddling, G. Mills, Current surface ozone concentrations significantly decrease wheat growth, yield and quality. *Sci. Total Environ.* **613-614**, 687–692 (2018).

2. E. A. Ainsworth, Understanding and improving global crop response to ozone pollution. *Plant J.* **90**, 886–897 (2017).

3. S. Avnery, D. L. Mauzerall, J. Liu, L. W. Horowitz, Global crop yield reductions due to surface ozone exposure: 2. Year 2030 potential crop production losses and economic damage under two scenarios of O_3 pollution. *Atmos. Environ.* **45**, 2297–2309 (2011).

4. E. A. Ainsworth, Rice production in a changing climate: A meta-analysis of responses to elevated carbon dioxide and elevated ozone concentration. *Glob. Chang. Biol.* **14**, 1642–1650 (2008).

5. E. A. Ainsworth, S. P. Serbin, J. A. Skoneczka, P. A. Townsend, Using leaf optical properties to detect ozone effects on foliar biochemistry. *Photosynth. Res.* **119**, 65–76 (2014).

6. A. Y. Khaled, S. A. Aziz, S. K. Bejo, N. M. Nawi, I. A. Seman, D. I. Onwude, Early detection of diseases in plant tissue using spectroscopy–applications and limitations. *Appl. Spectrosc. Rev.* **53**, 36–64 (2018).

7. F. Faoro, M. Iriti, Cell death behind invisible symptoms: Early diagnosis of ozone injury. *Biol. Plant.* **49**, 585–592 (2005).

8. W. Van Camp, H. Willekens, C. Bowler, M. Van Montagu, D. Inzé, P. Reupold-Popp, H. Sandermann Jr., C. Langebartels, Elevated levels of superoxide dismutase protect transgenic plants against ozone damage. *Biotechnol.* **12**, 165–168 (1994).

9. B. B. Moura, E. S. Alves, M. A. Marabesi, S. R. Souza, M. Schaub, P. Vollenweider, Ozone affects leaf physiology and causes injury to foliage of native tree species from the tropical atlantic forest of southern brazil. *Sci. Total Environ.* **610-611**, 912–925 (2018).

10. W. J. Massman, R. C. Musselman, A. S. Lefohn, A conceptual ozone dose-response model to develop a standard to protect vegetation. *Atmos. Environ.* **34**, 745–759 (2000).

11. L. D. Emberson, M. R. Ashmore, H. M. Cambridge, D. Simpson, J.-P. Tuovinen, Modelling stomatal ozone flux across europe. *Environ. Pollut.* **109**, 403–413 (2000).

12. E. Paoletti, A. Alivernini, A. Anav, O. Badea, E. Carrari, S. Chivulescu, A. Conte, M. L. Ciriani, L. Dalstein-Richier, A. De Marco, S. Fares, G. Fasano, A. Giovannelli, M. Lazzara, S. Leca, A. Materassi, V. Moretti, D. Pitar, I. Popa, F. Sabatini, L. Salvati, P. Sicard, T. Sorgi, Y. Hoshika, Toward stomatal–flux based forest protection against ozone: The MOTTLES approach. *Sci. Total Environ.* **691**, 516–527 (2019).

13. M. Jezek, A. Hills, M. R. Blatt, V. L. Lew, A constraint–relaxation–recovery mechanism for stomatal dynamics. *Plant Cell Environ.* **42**, 2399–2410 (2019).

14. S. Fares, A. Conte, A. Chabbi, Ozone flux in plant ecosystems: New opportunities for long-term monitoring networks to deliver ozone-risk assessments. *Environ. Sci. Pollut. Res.* **25**, 8240–8248 (2018).

15. M. H. Wong, J. P. Giraldo, S.-Y. Kwak, V. B. Koman, R. Sinclair, T. T. S. Lew, G. Bisker, P. Liu, M. S. Strano, Nitroaromatic detection and infrared communication from wild-type plants using plant nanobionics. *Nat. Mater.* **16**, 264–272 (2017).

16. S. Zhuang, L. Zhou, W. Xu, N. Xu, X. Hu, X. Li, G. Lv, Q. Zheng, S. Zhu, Z. Wang, J. Zhu, Tuning transpiration by interfacial solar absorber-leaf engineering. *Adv. Sci.* **5**, 1700497 (2018).

17. J. P. Giraldo, M. P. Landry, S. M. Faltermeier, T. P. McNicholas, N. M. Iverson, A. A. Boghossian, N. F. Reuel, A. J. Hilmer, F. Sen, J. A. Brew, M. S. Strano, Plant nanobionics approach to augment photosynthesis and biochemical sensing. *Nat. Mater.* **13**, 400 (2014).

18. S.-Y. Kwak, J. P. Giraldo, M. H. Wong, V. B. Koman, T. T. S. Lew, J. Ell, M. C. Weidman, R. M. Sinclair, M. P. Landry, W. A. Tisdale, M. S. Strano, A nanobionic light-emitting plant. *Nano Lett.* **17**, 7951–7961 (2017).

19. Y. Jie, X. Jia, J. Zou, Y. Chen, N. Wang, Z. L. Wang, X. Cao, Natural leaf made triboelectric nanogenerator for harvesting environmental mechanical energy. *Adv. Energy Materi.* **8**, 1703133 (2018).

20. Y. Chen, Y. Jie, J. Wang, J. Ma, X. Jia, W. Dou, X. Cao, Triboelectrification on natural rose petal for harvesting environmental mechanical energy. *Nano Energy* **50**, 441–447 (2018).

21. E. Stavrinidou, R. Gabrielsson, E. Gomez, X. Crispin, O. Nilsson, D. T. Simon, M. Berggren, Electronic plants. *Sci. Adv.* **1**, e1501136 (2015).

22. E. Stavrinidou, R. Gabrielsson, K. P. R. Nilsson, S. K. Singh, J. F. Franco-Gonzalez, A. V. Volkov, M. P. Jonsson, A. Grimoldi, M. Elgland, I. V. Zozoulenko, D. T. Simon, M. Berggren, In vivo polymerization and manufacturing of wires and supercapacitors in plants. *Proc. Natl. Acad. Sci. U.S.A.* **114**, 2807–2812 (2017).

23. D. J. Poxson, M. Karady, R. Gabrielsson, A. Y. Alkattan, A. Gustavsson, S. M. Doyle, S. Robert, K. Ljung, M. Grebe, D. T. Simon, M. Berggren, Regulating plant physiology with organic electronics. *Proc. Natl. Acad. Sci. U.S.A.* **114**, 4597–4602 (2017).

24. I. Bernacka-Wojcik, M. Huerta, K. Tybrandt, M. Karady, M. Y. Mulla, D. J. Poxson, E. O. Gabrielsson, K. Ljung, D. T. Simon, M. Berggren, E. Stavrinidou, Implantable organic electronic ion pump enables ABA hormone delivery for control of stomata in an intact tobacco plant. *Small* **15**, e1902189 (2019).

25. N. Coppedè, M. Janni, M. Bettelli, C. L. Maida, F. Gentile, M. Villani, R. Ruotolo, S. Iannotta, N. Marmiroli, M. Marmiroli, A. Zappettini, An *in vivo* biosensing, biomimetic electrochemical transistor with applications in plant science and precision farming. *Sci. Rep.* **7**, 16195 (2017).

26. J. J. Kim, L. K. Allison, T. L. Andrew, Vapor-printed polymer electrodes for long-term, on-demand health monitoring. *Sci. Adv.* **5**, eaaw0463 (2019).

27. V. B. Koman, T. T. S. Lew, M. H. Wong, S.-Y. Kwak, J. P. Giraldo, M. S. Strano, Persistent drought monitoring using a microfluidic-printed electro-mechanical sensor of stomata *in planta*. *Lab Chip* **17**, 4015–4024 (2017).

28. K. Lee, J. Park, M.-S. Lee, J. Kim, B. G. Hyun, D. J. Kang, K. Na, C. Y. Lee, F. Bien, J.-U. Park, In-situ synthesis of carbon nanotube–graphite electronic devices and their integrations onto surfaces of live plants and insects. *Nano Lett.* **14**, 2647–2654 (2014).

29. J. M. Nassar, S. M. Khan, D. R. Villalva, M. M. Nour, A. S. Almuslem, M. M. Hussain, Compliant plant wearables for localized microclimate and plant growth monitoring. *npj Flex. Electron.* **2**, 24 (2018).

30. G. Soja, M. Eid, H. Gangl, H. Redl, Ozone sensitivity of grapevine (*Vitis vinifera* L.): Evidence for a memory effect in a perennial crop plant? *Phyton* **37**, 265–270 (1997).

31. G. Soja, T. G. Reichenauer, M. Eid, A.-M. Soja, R. Schaber, H. Gangl, Long-term ozone exposure and ozone uptake of grapevines in open-top chambers. *Atmos. Environ.* **38**, 2313–2321 (2004).

32. A. Valletta, E. Salvatori, A. R. Santamaria, M. Nicoletti, C. Toniolo, E. Caboni, A. Bernardini, G. Pasqua, F. Manes, Ecophysiological and phytochemical response to ozone of wine grape cultivars of *Vitis vinifera* L. *Nat. Prod. Res.* **30**, 2514–2522 (2016).

33. T. Repo, E. Oksanen, E. Vapaavuori, Effects of elevated concentrations of ozone and carbon dioxide on the electrical impedance of leaves of silver birch (*Betula pendula*) clones. *Tree Physiol.* **24**, 833–843 (2004).

34. A. Martin, B. S. Chang, Z. Martin, D. Paramanik, C. Frankiewicz, S. Kundu, I. D. Tevis, M. Thuo, Heat-free fabrication of metallic interconnects for flexible/wearable devices. *Adv. Funct. Mater.* **29**, 1903687 (2019).

35. L. R. Thorne, Oxidation of Thin Silver Films by Ozone and Atomic Oxygen, in *Undergraduate Honors Capstone Projects* (1973), vol. 177.

36. J. M. Simmons, B. M. Nichols, S. E. Baker, M. S. Marcus, O. M. Castellini, C.-S. Lee, R. J. Hamers, M. A. Eriksson, Effect of ozone oxidation on single-walled carbon nanotubes. *J. Phys. Chem. B* **110**, 7113–7118 (2006).

37. T. Nagata, S. Oh, T. Chikyow, Y. Wakayama, Effect of UV-ozone treatment on electrical properties of PEDOT:PSS film. *Org. Electron.* **12**, 279–284 (2011).

38. X. Wang, X. Zhang, L. Sun, D. Lee, S. Lee, M. Wang, J. Zhao, Y. Shao-Horn, M. Dincă, T. Palacios, K. K. Gleason, High electrical conductivity and carrier mobility in oCVD PEDOT thin films by engineered crystallization and acid treatment. *Sci. Adv.* **4**, eaat5780 (2018).

39. M. Heydari Gharahcheshmeh, K. K. Gleason, Device fabrication based on oxidative chemical vapor deposition (oCVD) synthesis of conducting polymers and related conjugated organic materials. *Adv. Mater. Interfaces* **6**, 1801564 (2019).

40. O. G. Martinsen, S. Grimnes, *Bioimpedance and Bioelectricity Basics* (Academic press, 2011).

41. M. Grossi, B. Riccò, Electrical impedance spectroscopy (EIS) for biological analysis and food characterization: A review. *J. Sens. Sensor Syst.* **6**, 303–325 (2016).

42. A. Angersbach, V. Heinz, D. Knorr, Evaluation of process-induced dimensional changes in the membrane structure of biological cells using impedance measurement. *Biotechnol. Prog.* **18**, 597–603 (2002).

43. D. Tomkiewicz, T. Piskier, A plant based sensing method for nutrition stress monitoring. *Precis. Agric.* **13**, 370–383 (2012).

44. W. L. Chameides, The chemistry of ozone deposition to plant leaves: Role of ascorbic acid. *Environ. Sci. Technol.* **23**, 595–600 (1989).

45. X. Wei, J. Chen, Y. Yu, Z. Wang, H. Liu, D. Pan, J. Chen, Phylloremediation of air pollutants: Exploiting the potential of plant leaves and leaf-associated microbes. *Front. Plant Sci.* **8**, 1318 (2017).

46. J. N. Cape, Effects of airborne volatile organic compounds on plants. *Environ. Pollut.* **122**, 145–157 (2003).

47. J. J. Kim, T. L. Andrew, Real-time and noninvasive detection of UV-induced deep tissue damage using electrical tattoos. *Biosens. Bioelectron.* **150**, 111909 (2020).

48. Y. Ando, K. Mizutani, N. Wakatsuki, Electrical impedance analysis of potato tissues during drying. *J. Food Eng.* **121**, 24–31 (2014).

49. M. I. N. Zhang, J. H. M. Willison, Electrical impedance analysis in plant tissues11. *J. Exp. Bot.* **42**, 1465–1475 (1991).

50. C. H. Hsu, F. Mansfeld, Concerning the conversion of the constant phase element parameter Y_0 into a capacitance. *Corrosion* **57**, 747–748 (2001).